Journal of Computational Physics 231 (2012) 8100–8113

Contents lists available at SciVerse ScienceDirect

Journal of Computational Physics

journal homepage: www.elsevier.com/locate/jcp

Local–global multiscale model reduction for flows in high-contrast heterogeneous media

Yalchin Efendiev [a,*], Juan Galvis [a,b], Eduardo Gildin [c]

[a] Department of Mathematics, Texas A&M University, College Station, TX 77843, United States
[b] Departamento de Matemáticas, Universidad Nacional de Colombia, Carrera 30, calle 45, Ciudad Universitaria Bogotá, Colombia
[c] Department of Petroleum Engineering, Texas A&M University, College Station, TX 77843, United States

ARTICLE INFO

Article history:
Received 17 April 2011
Received in revised form 18 July 2012
Accepted 24 July 2012
Available online 9 August 2012

Keywords:
Multiscale
High contrast
Model reduction
Finite element
Balanced truncation

ABSTRACT

In this paper, we study model reduction for multiscale problems in heterogeneous high-contrast media. Our objective is to combine local model reduction techniques that are based on recently introduced spectral multiscale finite element methods (see [19]) with global model reduction methods such as balanced truncation approaches implemented on a coarse grid. Local multiscale methods considered in this paper use special eigenvalue problems in a local domain to systematically identify important features of the solution. In particular, our local approaches are capable of homogenizing localized features and representing them with one basis function per coarse node that are used in constructing a weight function for the local eigenvalue problem. Global model reduction based on balanced truncation methods is used to identify important global coarse-scale modes. This provides a substantial CPU savings as Lyapunov equations are solved for the coarse system. Typical local multiscale methods are designed to find an approximation of the solution for any given coarse-level inputs. In many practical applications, a goal is to find a reduced basis when the input space belongs to a smaller dimensional subspace of coarse-level inputs. The proposed approaches provide efficient model reduction tools in this direction. Our numerical results show that, only with a careful choice of the number of degrees of freedom for local multiscale spaces and global modes, one can achieve a balanced and optimal result.

1. Introduction

The high degree of variability and multiscale nature of heterogeneous porous media properties cause significant challenges for forward simulations. For this reason, some model reduction techniques are needed. Many multiscale and homogenization type methods are developed to provide an accurate representation of the solution. These approaches (e.g., [30,1,2,4,5,11,12,17,31,13,40,14,18,24,25,34,36,39]) approximate the effects of the fine-scale features and attempt to capture their effects on a coarse grid via localized basis functions. The main idea of the local multiscale methods is to construct basis functions that are used to approximate the solution on a coarse grid. Multiscale methods can be considered as local model reduction techniques that construct an approximation of the solution on a coarse grid for arbitrary coarse-level inputs. Our main goal is to use local model reduction techniques together with global ones in achieving efficient reduced-order approximations for input–output maps.

One of the earlier approaches in this direction is taken within the system theory framework [37,29,10,32,3]. In this setting, the system is written in terms of a mapping from input to output where the latter represents the quantity of interest for

* Corresponding author. Tel.: +1-979-458-0836.
E-mail address: efendiev@math.tamu.edu (Y. Efendiev).

0021-9991/$ - see front matter © 2012 Elsevier Inc. All rights reserved.
http://dx.doi.org/10.1016/j.jcp.2012.07.032

assessing the accuracy of the approximation. Input signals are regarded as quantities that we are controlling and output signals are the quantity that we are measuring. Characterizing the system by its input–output relation leads to the idea of state-space representation of the dynamical system, and in turn, to approximations by projecting the states to a smaller state-space dimension. The central issue in model reduction is, therefore, how to obtain efficiently the projection matrices, so that we preserve in the reduced-order models a small set of states that are relevant to the input–output behavior of the system. Approaches such as balanced truncation and proper orthogonal decompositions (POD) type techniques are proposed to perform global model reduction.

In this paper, we discuss how to combine efficient multiscale methods on a coarse grid with global model reduction techniques. We propose a model reduction technique that combines both local and global model reduction tools. We use the recently introduced local model reduction tools [19] that allow systematically identifying important degrees of freedom of the solution. These approaches allow lumping many degrees of freedom that can be localized as in homogenization. These local reduced models are combined with model reduction techniques on a coarse grid (that is inexpensive) to achieve an ultimate reduced model with fewer degrees of freedom. The resulting reduced model provides robust approximation of the global system at a substantially lower cost when the input belongs to a subset of all coarse-level functions.

In this paper, the balanced truncation method is used to reduce the global coarse-scale model. In the balanced truncation framework, one is interested in truncating simultaneously the states that are weakly controllable and weakly observable. This is accomplished by solving (coarse-scale) Lyapunov equations for the observability and controllability Gramians and computing the eigenvalues and eigenvectors of the product of Gramians. In the balanced truncation, one can obtain a priori bound for the error from the full system to the reduced system. Combining this bound with a priori error bound for coarse-grid multiscale approximation, we can achieve a reduced model with a prescribed accuracy. The accuracy of the proposed approach can be improved by adding local degrees of freedom as well as global degrees of freedom simultaneously. This is discussed in the paper.

We note that the use of approximate models in global model reduction methods such as within balanced truncation or POD approaches are not new. In many previous findings, various proxy models are used to make the model reduction affordable. Our main contribution is the use of systematic local model reduction methods that allow adding new degrees of freedom on a coarse-grid level. Moreover, our local approaches are capable of approximating the solution for any coarse-level inputs and thus the proposed methods will be efficient when the input belongs to a smaller dimensional space, e.g., the forcing or boundary conditions are defined only on a few coarse-grid blocks. Furthermore, our local approaches provide minimum degrees of freedom for high-contrast multiscale flow problems (see [19]), and thus the overall approach is efficient. The error estimates both on local and global model reduction methods allow obtaining a priori error estimates for the overall method.

Our approaches share similarities with reduced basis approaches [8,26,27,35] that can be considered as an umbrella approach for the techniques proposed here. The main idea of reduced basis approach is to select a number of snapshots that can be used to construct a basis for the solution space. In our approach, these snapshots are chosen on a coarse grid with some special choices of multiscale interpolation operators. In a paper by Krogstad [33], local POD techniques in combination with global solutions are used to construct multiscale basis functions. These methods approximate the local features of the solution using both global and local problems. These approaches differ from the ones proposed in our paper. In [16], the authors apply POD type methods together with coarse-scale models based on single-phase upscaling; however, these techniques only use single-phase permeability upscaling and the issues of enriching coarse spaces to balance the global and local model reduction errors are not investigated.

We present numerical results for flow problems in high-contrast multiscale media. We vary the dimensions of both local coarse spaces and global reduced space. We present the errors between fine-scale solution and corresponding coarse-scale solution and between coarse-scale solution and corresponding reduced coarse-scale solution obtained using some number of important modes of balanced truncation method. Our numerical results show that these errors can be comparable suggesting one needs to carefully select the coarse space when performing model reduction on the coarse system.

The paper is organized as follows. In the next section, we discuss the problem setting and local multiscale approximations. We present some preliminaries in Section 2. Section 3 is devoted to local–global multiscale model reduction. In particular, some remarks are discussed in Section 3.1. In Section 4, we present numerical results. Conclusions and final comments are presented in Section 5.

2. Preliminaries

We will demonstrate our methodology on an example of time-dependent single-phase flow, though the proposed method can be extended to other equations. For simplicity, we consider the following system where, for given input $u \in \mathbb{R}^m$, we seek of state $p(t,\cdot) \in H^1(D)$

$$\frac{\partial p}{\partial t} = \operatorname{div}(\kappa(x)\nabla p) + f(u) \in D. \tag{1}$$

Here $D \subset \mathbb{R}^2$ (or $\mathbb{R}^3$) and for every input (or control) $u \in \mathbb{R}^m$, the forcing $f(u)$ is a linear functional of u and it is assumed to be square integrable. In many applications, we are interested in achieving model reduction that provide an accurate

approximation for some observable quantity. Assume the observed quantity or output is $q \in \mathbb{R}^n$ that is given by an operator acting on the state p as

$$q = \mathcal{C}p. \tag{2}$$

Here $\mathcal{C}(p) = (\mathcal{C}_1(p), \ldots, \mathcal{C}_n(p))$, where $\mathcal{C}_i$ is a functional acting on functions in $H^1(D)$, $i = 1, \ldots, n$. The operator $\mathcal{C}$ will be referred to as state-to-output operator.

We assume $\kappa(x)$ is a heterogeneous field with a high contrast, i.e., the ratio $\max \kappa(x)/\min \kappa(x)$ is very large. In particular, we assume that κ is bounded away from zero ($\kappa(x) \geqslant c_0 > 0$), while $\kappa(x)$ can have very large values. We introduce the bilinear forms $\mathcal{S}$ and $\mathcal{T}$ and the linear functional $\mathcal{F}$ defined by

$$\mathcal{S}(p, w) = -\int_D \kappa(x)\nabla p(x) \cdot \nabla w(x)dx \quad \text{for all} \quad p, w \in H_0^1(D), \tag{3}$$

$$\mathcal{T}(p, w) = \int_D p(x)w(x)dx \quad \text{for all} \quad p, w \in H_0^1(D) \tag{4}$$

and

$$\mathcal{F}(w; u) = \int_D f(u)(x)w(x)dx \quad \text{for all} \quad w \in H_0^1(D).$$

The variational form of (1) is: find $p(t, x) \in C^0([0, T]) \times H_0^1(D)$ such that

$$\mathcal{T}\left(\frac{\partial p}{\partial t}, w\right) - \mathcal{S}(p, w) - \mathcal{F}(w; u) = 0 \quad \text{for all} \quad w \in H_0^1(D). \tag{5}$$

2.1. Local multiscale approach. Coarse-grid solution procedure that captures fine-scale resolution

We briefly recall the results for multiscale finite element methods for elliptic equation (see [19]). Let $\mathcal{T}^h$ be a fine triangulation, which is a refinement of $\mathcal{T}^H$, where $\mathcal{T}^H = \{K\}$ is a coarse-grid partition and H denotes the size of the coarse grid. We denote by $V^h(D)$ the usual space of finite element discretization of piecewise linear continuous functions with respect to the fine triangulation $\mathcal{T}^h$. We denote by $V_0^h(D)$ the subset of $V^h(D)$ with vanishing values on ∂D. The semi-discrete Galerkin formulation of (5) is to find $p(t, \cdot) \in V_0^h(D)$ such that

$$\mathcal{T}\left(\frac{\partial p}{\partial t}, w\right) - \mathcal{S}(p, w) - \mathcal{F}(w; u) = 0 \quad \text{for all } w \in V_0^h(D), \tag{6}$$

or in matrix form (for simplicity, we use the same notations for continuous and corresponding discrete quantities)

$$T\frac{\partial p}{\partial t} = Sp + Fu, \tag{7}$$

where for all $p, q \in V^h(D)$ we have

$$p^T Sq = \int_D \kappa \nabla p \nabla q, \quad p^T Tq = \int_D pq \quad \text{and} \quad q^T Fu = \int_D f(u)q. \tag{8}$$

We denote by $\{y_i\}_{i=1}^{N_v}$ the vertices of the coarse mesh $\mathcal{T}^H$ and define the neighborhood of the node y_i by

$$\omega_i = \bigcup \{K_j \in \mathcal{T}^H;\ y_i \in \overline{K}_j\}. \tag{9}$$

Using the coarse mesh $\mathcal{T}^H$ we introduce coarse basis functions $\{\Phi_i\}_{i=1}^{N_c}$ (see Fig. 1 for illustration), where N_c is the number of coarse basis functions. At this point, we keep the basis functions to be general partition and supported in ω_l's; however, for ω_l, there may be multiple basis functions. Given coarse-scale basis functions the coarse space is given by

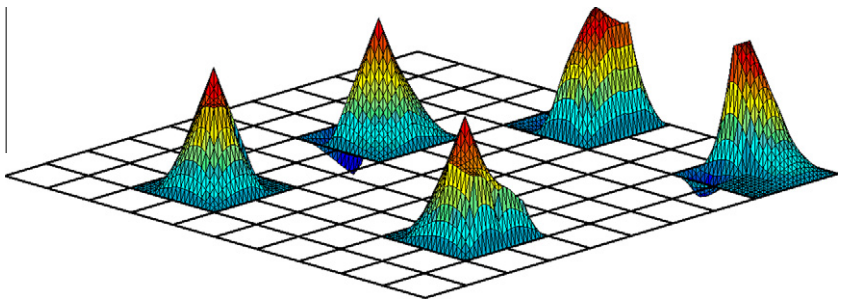

Fig. 1. Initial multiscale basis function.

$$V_0 = \text{span}\{\Phi_i\}_{i=1}^{N_c} \tag{10}$$

and the coarse matrices by $S_0 = R_0 S R_0^T$ and $T_0 = R_0 T R_0^T$, where

$$R_0^T = [\Phi_1, \ldots, \Phi_{N_c}].$$

Here Φ_i's are discrete coarse-scale basis functions defined on a fine grid (i.e., vectors). MsFEMs approximate the solution on the coarse space, i.e., we seek for approximation of $u_0 \in V_0$.

Once initial multiscale basis functions are constructed, we design a local spectral problem that is used to complement the initial coarse space. In particular, in each coarse block neighborhood we perform a local model reduction to identify important modes based on local elliptic energies. Furthermore, we multiply the local modes by a partition of unity so they become globally defined basis functions with local support. This procedure is briefly discussed below.

To define the coarse space we perform a local model reduction for each coarse block neighborhood. That is, in each block we identify important modes that represent the media properties. In this local model reduction, we will identify important basis functions based on a local elliptic energy inner product. More precisely, to define the coarse space we consider high-contrast eigenvalue problem following [22]. We start with an initial coarse space $V_0^{initial} = \text{span}\{\tilde{\chi}_i\}$. We consider $\tilde{\kappa}$ given by

$$\tilde{\kappa} = \kappa \sum_{i=1}^{N_v} H^2 |\nabla \tilde{\chi}_i|^2 \tag{11}$$

assuming κ is a scalar field ($\kappa \nabla \tilde{\chi}_i \cdot \nabla \tilde{\chi}_i$ is used when κ is a tensor). This is the pointwise energy for basis functions computed by summing all basis function energies. Once $\tilde{\kappa}$ is defined, we propose the following homogeneous Neumann eigenvalue problem in each coarse block neighborhood ω,

$$-\text{div}(\kappa \nabla \psi_\ell) = \lambda_\ell \tilde{\kappa} \psi_\ell \tag{12}$$

and denote its eigenvalues and eigenvectors by $\{\lambda_\ell^\omega\}$ and $\{\psi_\ell^\omega\}$, respectively. Note that the eigenvectors $\{\psi_\ell^\omega\}$ form an orthonormal basis of $V^h(\omega)$ with respect to the inner products defined via $\int_\omega \kappa(x) \nabla \psi_i^\omega \cdot \nabla \psi_j^\omega$ and $\int_\omega \tilde{\kappa}(x) \psi_i^\omega \psi_j^\omega$.

Remark 1. The eigenvalue problem above and the special weight $\tilde{\kappa}$ are motivated by abstract domain decomposition theory and multiscale techniques. We mention that this eigenvalue problem is also related to contrast-independent Poincaré inequalities of the form $\int_D \tilde{\kappa} v^2 \leqslant C \int_D \kappa |\nabla v|^2$, (with C independent of the contrast) that appear naturally in the analysis of robust domain decomposition and multiscale methods. In multiscale methods (see [19]), the error can be written as

$$\int_D \kappa |\nabla (u - u^{ms})|^2 \preceq \sum_i \int_{\omega_i} \kappa |\chi_i|^2 |\nabla (u - u_0)|^2 + \sum_i \int_{\omega_i} \kappa |\nabla \chi_i|^2 |(u - u_0)|^2,$$

where u_0 is the local approximation of the solution in ω_i generated using eigenfunctions corresponding to smallest eigenvalues. In this error estimate, one can bound the second term by the first one which gives the form of the eigenvalue problem. This motivates the eigenvalue problem and the fact that the initial multiscale basis functions need to be chosen such that to minimize their energies. We propose the use of multiscale finite element basis functions and discuss what will be corresponding dimension reduction for high-contrast media consisting of inclusions and channels. This choice of initial basis function allows eliminating many small eigenvalues. For further details on the derivation and analysis of (12) we refer to [19–23].

We order eigenvalues as

$$\lambda_1^\omega \leqslant \lambda_2^\omega \leqslant \cdots \leqslant \lambda_\ell^\omega \leqslant \cdots. \tag{13}$$

Note that $\lambda_1^\omega = 0$. In general, if $\tilde{\kappa}$ has m inclusions and channels, then one can observe m small, asymptotically vanishing, eigenvalues (see e.g., [19]). The eigenvectors corresponding to these eigenvalues will be used to construct the coarse space V_0. We choose the basis functions that span the eigenfunctions corresponding to small, asymptotically vanishing, eigenvalues in the way described below. Define the set of coarse basis functions (see Fig. 2 for illustration)

$$\Phi_{i,\ell} = \tilde{\chi}_i \psi_\ell^{\omega_i} \quad \text{for} \quad 1 \leqslant i \leqslant N_v \text{ and } 1 \leqslant \ell \leqslant L_i, \tag{14}$$

where L_i is the number of eigenvalues that will be chosen for the node i; see [6,38] for more details on the generalized finite element method using partitions of unity. Denote by V_0, as before, the *local spectral multiscale* space

$$V_0 = \text{span}\{\Phi_{i,\ell} : 1 \leqslant i \leqslant N_v \quad \text{and} \quad 1 \leqslant \ell \leqslant L_i\}. \tag{15}$$

The choice of partition of unity functions $\tilde{\chi}_i$ is important [23,22,20,19]. In particular, with a choice of initial basis functions, we attempt to capture as much local features of the solution as possible. Then, extra basis functions represent the features that are not captured by initial basis functions.

Next, we briefly discuss approximation properties of coarse spaces. Because of the Galerkin finite element formulation used on a coarse grid, in [19], we show that the convergence rate

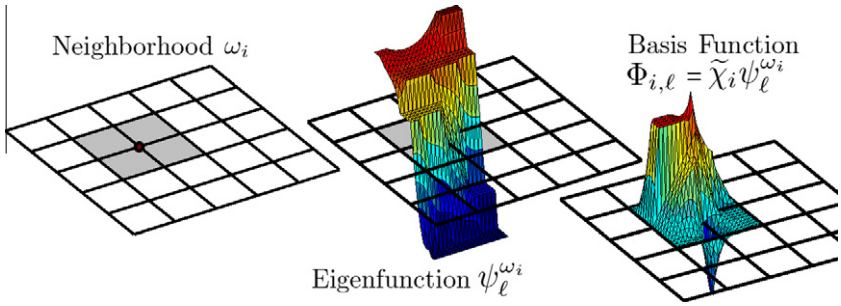

Fig. 2. Illustration of spectral multiscale basis construction.

$$\int_D \kappa |\nabla(p - p_0)|^2 \preceq \frac{H^{1+\beta}}{\Lambda_*}, \tag{16}$$

where

$$\Lambda^* = \min_{1 \leqslant i \leqslant N_v} \lambda_{L_i+1}$$

is the minimum eigenvalue that is not included in the coarse space and $\beta \geqslant 0$ represents smoothness of the solution of the elliptic equation. The convergence rate estimate does not make any specific assumption on the initial partition of unity functions. However, by minimizing (11), one obtains smaller eigenvalues for a given dimension of the coarse space. The choice of the partition of unity functions is essential for the construction of multiscale basis functions. The objective is to achieve larger Λ_* with smaller coarse spaces. For this reason, we choose initial multiscale basis functions to approximately minimize (11) and thus remove small eigenvalues rapidly. With a good choice of initial multiscale basis functions, we incorporate all the features that can be localized into one basis function per node. We note that multiscale finite element methods presented above are designed to approximate the solution for any coarse-level input data, such as forcing or boundary conditions.

2.2. Global model reduction

We recall that, given p, the output q can be computed as $q = Cp$. We rewrite problem (7)

$$\begin{aligned} &\tfrac{d}{dt} p = Ap + Bu \\ &q = Cp. \end{aligned} \tag{17}$$

Here p denotes the discrete solution (e.g., discretized by Galerkin FEM) or the states of the dynamical system, $A = T^{-1}S$ where T and S are defined in (8), $B = T^{-1}F$ and C is the matrix representation of the state-to-output operator $\mathcal{C}$ and it is given by $Cp = \mathcal{C}(p)$ for all $p \in V^h(D)$. In practical applications $\mathcal{C}$ may be related to a coarse triangulation which may be independent of the coarse triangulation $\mathcal{T}^H$ used to construct the locally spectral coarse space in Section 2.1.

Assume that the fine grid discretization has N degrees of freedom, so A is an $N \times N$ matrix. We assume that $u \in \mathbb{R}^m$ and $q \in \mathbb{R}^n$. In some practical applications, the input u is defined using a coarse grid with m grid blocks while q is defined on a (maybe different) coarse grid with n grid blocks. In general, we can take $m = n$. Then, B is $N \times n$ matrix, while C is $m \times N$ matrix. According to (10), the dimension of the coarse discretization is N_c. We assume also that $m \leqslant N_c$ and $n \leqslant N_c$.

We briefly review global model reduction from the point of view of system theory where more general systems are typically studied. The relation between inputs and outputs from (17) is usually analyzed in the frequency domain, or the Laplace domain, by means of the transfer function of the dynamical system, namely, $G(s) = C(sI - A)^{-1}B$. In this case, s is a complex variable used to obtain the Laplace transform of the differential equation, and $Q(s) = G(s)U(s)$ represents the input–output relation, where $Q(s)$ and $U(s)$ are Laplace transforms of q and u.

The internal description of the dynamical system by means of a state-space representation, as in (7), allows one to assess the importance of the states, p, by means of inputs, u and outputs, q. In general, they are related by the introduction of two fundamental ideas: controllability and observability. The reader can refer to [3] for further explanations.

An important definition, related to the controllability and observability matrices, is the concept of infinite Gramians and its relation to Lyapunov equations; see [3]. The so-called infinite reachability (controllability) Gramian $\mathcal{P}$ and the infinite observability Gramian $\mathcal{Q}$ are theoretically defined as

$$\mathcal{P} = \int_0^\infty e^{A\tau}\, BB^T e^{A^T\tau} d\tau \quad \text{and} \quad \mathcal{Q} = \int_0^\infty e^{A^T\tau}\, C^T\, Ce^{A\tau} d\tau. \tag{18}$$

It readily follows that $\mathcal{P}$ and $\mathcal{Q}$ are symmetric and positive semidefinite. Moreover the infinite Gramians satisfy the following coupled Lyapunov equations,

$$A\,\mathcal{P}+\mathcal{P}\,A^T+\,BB^T=\,0\quad\text{and}\quad A^T\mathcal{Q}+\mathcal{Q}\,A+\,C^T\,C=\,0. \tag{19}$$

The importance of the the controllability and observability Gramians stems from its relation to the smallest amount of energy necessary to steer a state from, say zero initial conditions, to a final state, p and to the amount of energy obtained by observing the output, with initial conditions p and no external excitation, respectively.

One of the most effective global model reduction techniques is *Balanced Truncation*; see [3]. By analyzing the eigenvalues associated with the two Gramians, one can readily assemble a reduced-order model by eliminating the states which require a large amount of energy to be reached and/or yield small amounts of observation energy. The main issue here, however, is that the two Gramians are basis-dependent and care must be taken when truncating states. Working with each Gramian independently, one does not guarantee that the remaining (after truncation) states are simultaneously strongly controllable and observable.

A way to overcome this difficulty is to look for basis such that the two Gramians are equivalent. This leads to the concept of balanced basis. A state-space transformation is then derived to balance the system in the sense that the two Gramians become diagonal and equal. In this new coordinate system, states that are difficult to reach are simultaneously difficult to observe. This can be seen by the fact that, in the balanced basis, the Gramians are given by $diag(\sigma_1,\ldots,\sigma_L)$, where the $\sigma_i=\sqrt{\lambda_i(\mathcal{PQ})}$ for $i=1,\ldots,L$, are the so-called Hankel Singular Values (HSV) of the dynamical system. The HSV in this case, define a measure of the accuracy of the approximation. In most cases, the HSV decays fast and reduced-order models of smaller sizes can be obtained. One of the main advantages of balanced truncation is the existence of a priori error bound for the difference between the original model response, or transfer function, $G(s)$ and the reduced order model response, written here in a compact form, $G_r(s)=\left[\begin{array}{c|c}\tilde{A}&\tilde{B}\\\hline\tilde{C}&0\end{array}\right]$ obtained by balanced truncation. One can show that the error bound satisfies

$$\|G(s)-\,G_r(s)\|_{\mathcal{H}_\infty}\preceq\left(\sigma_{k+1}+\cdots+\sigma_q\right), \tag{20}$$

where $\|G\|_\infty=ess\sup_{\omega\in\mathbb{R}}\sigma(G(i\omega))$ with $i=\sqrt{-1}$ and $s=i\omega$. See [42] and references therein.

Other important issues to mention about the reduced order models obtained by balanced truncation are: (1) given a stable system to begin with, that is, A have eigenvalues in the left half of the complex plane, the reduced models are guaranteed to be stable, and thus, the solution converges to a steady-state; (2) the reduced models are balanced and minimal, that is, their Gramians are equal and diagonal and they are guaranteed to be controllable and observable; finally, (3) connections with POD. The latter will be discussed later in the paper, but now it suffices to say that in the linear system framework, balanced truncation is a POD method combined with a Petrov–Galerkin projection applied to the impulsive response of the system [41].

3. Local–global multiscale model reduction

In this section, we discuss how local and global approaches can be combined to achieve a flexible local–global model reduction framework for multiscale problems. Practical applications of balanced truncation relies on computing the solution of the two coupled Lyapunov equations in (19) to obtain the controllability and observability Gramians $\mathcal{P}$ and $\mathcal{Q}$, respectively. Moreover, after $\mathcal{P}$ and $\mathcal{Q}$ are computed, an eigenvalue problem $\mathcal{PQ}X=X\Sigma$ needs to be solved. Although balanced truncation yields reduced order models with desired properties, the main computational bottle neck is how one can efficiently compute the two coupled large dimension Lyapunov equations. In the linear systems framework, the cost of evaluating the two large-scale Lyapunov equations is of order $\mathcal{O}(N^3)$ and memory storage of $\mathcal{O}(N^2)$. Although in recent years [7] many advances in mitigating the computational effort have been implemented, specially using concepts of low rank approximations of matrices [7,3], their solution in the large-scale setting is still a major drawback for practical application of balanced truncation procedures to problems with large dimensional state spaces. In the nonlinear framework, however, POD relies on the simulation of the dynamical system as many times as necessary to capture all the spectrum of the excitation frequencies. Thus, the main computational burden is the solution of the forward problem l times, where l is a problem dependent variable, which reflects time span and input spaces.

By using an appropriate multiscale formulation, we can overcome this issue in a satisfactory way. In the new proposed local–global model reduction, instead of applying the balanced truncation method directly to the high-dimensional fine resolution model (7) we apply it to a smaller dimensional coarse scale model. Instead of model (7) we consider a coarse multiscale model. In this case, we need to solve only a small dimensional Lyapunov equation. The multiscale model to be used instead of the fine scale model (7) employs the space V_0 defined in (10) whose construction involves local POD model reduction; see Section 2.1. Next, we present more details of the local–global model reduction procedure.

We will use local spectral multiscale finite element methods (MsFEM) to construct the coarse system to which the balanced truncation method will be applied. In this regard, our approach can be thought as performing global model reduction on a coarse grid that is inexpensive. The main point here is to show that with a limited number of degrees of freedom on a coarse grid and for a global system, we can achieve a desired tolerance. Because our approaches select a minimum degrees of freedom on a coarse grid and consequently the same holds for a global problem, the proposed approach is efficient and robust.

Multiscale finite element solution is the finite element projection of the fine-scale solution into the space V_0. The solution of this equation can be written as

$$\frac{dp_0}{dt} = A_0 p_0 + B_0 u, \tag{21}$$

where $A_0 = T_0^{-1} R_0 S R_0^T$, $T_0 = R_0 T R_0^T$ and $B_0 = R_0 B$. The output q_0 can be computed by

$$q_0 = C_0 p_0, \tag{22}$$

where $C_0 = C R_0^T$.

We will perform balanced truncation on a coarse system described by (21) and (22). For this reason, we write the coarse model response as

$$G_0(s) = \left[\begin{array}{c|c} A_0 & B_0 \\ \hline C_0 & 0 \end{array}\right] \tag{23}$$

Next, we use balanced truncation to determine a reduced model for appropriate coarse-scale system where the number of basis functions are still not determined. The reduced system is found by considering the balanced truncation procedure described earlier applied to the coarse scale model (21) and (22). The corresponding coarse scale Lyapunov equations are,

$$A_0\ \mathcal{P}_0 + \mathcal{P}_0\ A_0^T + \ B_0 B_0^T = \ 0 \quad \text{and} \quad A_0^T \mathcal{Q}_0 + \mathcal{Q}_0\ A_0 + \ C_0^T\ C_0 = \ 0. \tag{24}$$

As before we compute a basis that transforms the controllability and observability Gramians, $\mathcal{P}_0, \mathcal{Q}_0$, respectively, to be equal and diagonal [3]. In this case, the quantities $\sigma_i^0 = \sqrt{\lambda_i(\mathcal{P}_0 \mathcal{Q}_0)}$, $i = 1, \cdots, n$ are defined as the Hankel Singular Values of the coarse system. The reduced system on a coarse grid is obtained by selecting the dominant eigenvalues and its response is $G_0^r(s) = \left[\begin{array}{c|c} \tilde{A}_0 & \tilde{B}_0 \\ \hline \tilde{C}_0 & 0 \end{array}\right]$. As before, we have the error bound

$$\|G_0(s) - \ G_r^0(s)\|_{\mathcal{H}_\infty} \preceq \left(\sigma_{k+1}^0 + \cdots + \sigma_q^0\right). \tag{25}$$

Next, we combine the error estimates for multiscale methods and balanced truncation for coarse-scale system. We denote the output corresponding to the reduced system by q_0^r and the output obtained by coarse-scale approximation by q_0. Using triangular inequality, we have

$$\int_0^T \|q - q_0^r\|^2 dt \preceq \int_0^T \|q - q_0\|^2 dt + \int_0^T \|q_0 - q_0^r\|^2 dt. \tag{26}$$

As we discussed earlier, using additional local basis functions can improve the first term on the right-hand side while using global coarse-scale modes can improve the second term on the right-hand side. The estimate for the first term can be obtained by MsFEM studies. Here, we use the estimate obtained for elliptic systems as the underlying problem does not have any temporal scales. We will show them numerically in the next section. The error can be written as

$$\int_0^T (p - R_0 p_0)^T S (p - R_0 p_0) dt = \int_0^T \|p - R_0 p_0\|_S^2 dt \preceq \max_i \frac{H^{1+\beta}}{\lambda_{L+1}^i},$$

where i denotes the coarse grid block number and λ_{L+1}^i is the eigenvalue for which the corresponding eigenvectors are not included in the coarse space and S is the stiffness matrix defined in (3). To estimate the error in the output, we note

$$\|q - q_0\|^2 = \|C(p - R_0 p_0)\|^2 \leqslant \|C\|_S \|p - p_0\|_S^2,$$

where $\|C\|_S = \sup_z (Cz, Cz)/(Sz, z)$. Then,

$$\int_0^T \|q - q_0\|^2 dt \preceq \|C\|_S \int_0^T \|p - p_0\|_S^2 \preceq \|C\|_S \max_i \frac{H^{1+\beta}}{\lambda_{L+1}^i}. \tag{27}$$

On the other hand, based on the accuracy of balanced truncation (cf.(20) and Chapter 4 of [42]), we have

$$\int_0^T \|q_0 - q_0^r\|^2 dt \preceq (\sigma_{k+1}^0 + \ldots + \sigma_l^0). \tag{28}$$

Combining the previous estimates (27) and (28), we obtain

$$\int_0^T \|q - q_0^r\|^2 dt \preceq \|C\|_S \frac{H^{1+\beta}}{\lambda_{L+1}^i} + (\sigma_{r+1}^0 + \ldots + \sigma_l^0).$$

As we see from this estimate that if C introduces a norm weaker than S, then one can assume that $\|C\|_S \preceq 1$. Note that these estimates can be extended to time-dependent smooth source terms (cf. [28]).

3.1. Remarks

As we observe from the above error estimates one needs to carefully balance coarse-grid solution error and global model reduction error. Our numerical results show that one error can dominate the other depending on the global flow scenario. A judicious choice of coarse-grid approximation and an appropriate number of Hankel Singular Values needs to be selected. As we mentioned the use of approximate models within global model reduction methods is not new. Many approaches employ simplified models to perform forward calculations. The main advantages of the proposed methods are (1) they allow systematically adding new degrees of freedom on a (local) coarse-grid level (2) they can provide an accurate approximation for any coarse-level input at a small cost by incorporating localizable features into one basis functions (3) there are a priori convergence rates that allow balancing the local and global errors.

We note that our coarse-grid solution provides an accurate approximation in the energy norm. In our analysis, we assumed the output error can be bounded by the energy error in the solution. This is true for our numerical examples where we select the output to be the average of the solution. However, this may not hold for certain quantities. In this case, we will need to use special test functions that can provide robust approximation in a desired norm [15].

In the proposed approach, as a first step, we select model reduction on a coarse grid and further reduction is taken place on a global coarse model. An open question is whether one can design coarse-grid model (multiscale basis functions) directly based on the output space (cf. [16]).

We mention that our proposed approaches can be applied in conjunction with POD methods. In POD methods, the snapshots of the solutions are constructed by solving the forward problem for a set of input functions. Furthermore, POD-type approach is applied to identify basis functions in the space of snapshots. The relation between these approaches are demonstrated in [41]. In particular, it was shown that POD eigenvectors for an extensive snapshot set are the eigenvectors of the controllability Gramian corresponding to largest eigenvalues. To use the proposed techniques within POD approaches, we will solve l forward coarse-scale solutions on a coarse grid using an appropriate number of basis functions. Denote these outputs by $p_0^{(1)}(t), \ldots, p_0^{(l)}(t)$. We note that the basis functions are constructed once for all forward computations and this can provide a substantial speed-up. Furthermore, using POD methods, we identify the best basis that represents these snapshots on a coarse grid in an appropriate space–time norm (see e.g., [41]).

As mentioned before, balanced truncation becomes impractical for large-scale systems. The bottleneck is the large-scale Lyapunov equations associated with balancing the system and the fact that the whole state-space is needed to compute the projection matrices. In addition, balanced truncation cannot be easily applied to nonlinear systems. As an alternative, POD-like methods can be used instead. The classical POD method is simple to use and may not require any major computational effort. It requires a training solution to be computed offline, and some saved snapshots at particular discrete time steps. The major drawback stems from the fact that there is not a known set of training inputs and discrete time steps to properly account for all the dynamics to be captured in the reduced-order model.

In many subsurface applications, there are nonlinearities due to changing flow conditions in time and one needs to update basis functions at different time instants. For example, in [9], the authors use POD-based model reduction techniques for solving multi-phase flow and transport by taking the snapshots of the solution at different time instants.

Several authors extended the balanced truncation method to the nonlinear case using ideas from the POD scheme. Rather than solving the Lyapunov equations entirely, one can approximate the Gramians by using the so-called snapshot-based Gramians, or empirical Gramians, in which data from numerical simulation (training data) is used to compute directly the Gramians. The drawbacks of empirical Gramians are two fold: first, the approximation is performed using discrete time sampling to a continuous definition of varying impulse responses. Then, there is a truncation to the infinity integration limit of the Gramian. If the high-frequencies modes decay fast, this source of error is minimal. However, there is not an easy answer when this is applied to large-scale nonlinear systems. The modes may be hard to compute. An alternative is to use the a variant called the Balanced POD. Again, this method relies on the snapshot matrices computed previously and carry on the same type of approximation errors.

As seen previously, in the nonlinear setting, POD and the balanced truncation methods can be applied by constructing snapshots of the solutions. With our proposed approaches, the space of snapshot can be inexpensively computed by solving the forward problem on a coarse grid. However, because one needs to project back to the high dimensional space in order to evaluate the nonlinear terms at every time step, the overall procedure can be expensive. To overcome this burden, two other techniques can be used, namely the trajectory piece-wise linearizion (TPWL) and the discrete empirical interpolation method (DEIM), which basically, perform linearizations of the nonlinear system in particular states of the dynamical system. The TPWL has been applied recently in the context of porous media flow. The main idea of POD-DEIM is to overcome the computational burden of projecting the nonlinear system back to the full-order dimension by means of interpolation of the nonlinear factors (nonlinear snapshots). In this case, one computes snapshots of the nonlinear terms of the equations, in addition to the states, and finds a new interpolation projection basis which reduces the dimensions of the nonlinear terms directly. We are working on extensions of the proposed methods by considering local reduced-order models for the interpolation states of the dynamical system and for the overall procedure.

The proposed approaches can benefit from a choice of a coarse grid. By choosing coarse regions adaptively, one can reduce the number of degrees of freedom needed to represent local features of the solution. However, in many applications, such as porous media, the choice of the coarse grid may come from a discretization of other equations in a coupled system or can

have geometrical constraints. Our proposed approaches are designed to provide minimal degrees of freedom for any choice of the coarse mesh.

In the future, we plan to investigate combining the proposed methods with the approaches developed in [9] to address time-dependent heterogeneities that arise in multi-phase simulations.

4. Numerical results

In this section, we present some representative numerical results. The global domain is taken to be $D = [0,1] \times [0,1]$. The fine mesh is taken to be 100×100. The coarse-mesh size is taken to be 10×10 or 20×20. We assume that the forcing f is piecewise constant function on a coarse grid, and thus B is a block diagonal matrix consisting of ones that maps piecewise constant function on a coarse grid to the fine grid. We take C to be the transpose of B in our numerical examples. We assume homogeneous Dirichlet boundary conditions.

We will use local multiscale basis functions with different number of basis functions. We choose the following notation: LSM+n indicates that the coarse spaces that include eigenvectors corresponding to small, asymptotically vanishing eigenvalues (see e.g., [19]) and additional n eigenvectors corresponding to the next n eigenvalues (in an increasing order). E.g., LSM+0 indicates the coarse space that only includes eigenvectors corresponding to small, asymptotically vanishing eigenvalues, while LSM+1 indicates the coarse space that includes eigenvectors corresponding to small, asymptotically vanishing eigenvalues, plus one more eigenvector in each coarse region that corresponds to the next largest eigenvalue. In our numerical examples, we consider high-contrast permeability fields.

In our numerical simulations, we will take different number of Hankel Singular Values (HSV) for global coarse model reduction. After truncating the global coarse system, we will use these basis for solving the problem for some chosen force function and compare the error between fine-scale solution and coarse-scale solution and the error between coarse-scale solution and the reduced coarse-scale solution. Our numerical results show that one needs to carefully select the number of HSVs and the number of multiscale basis functions (i.e., the dimension of the coarse space). The numerical results are sensitive to a choice of forcing term and we will discuss it in the paper.

4.1. Example 1

In our first numerical example, we use the coefficient depicted in Fig. 3 that corresponds to a coefficient with background one and high conductivity (denoted by η) channels and inclusions within each region. We use two different source terms and present errors. In Table 1, numerical results are presented when the force term that is 1 in the whole domain. The solutions

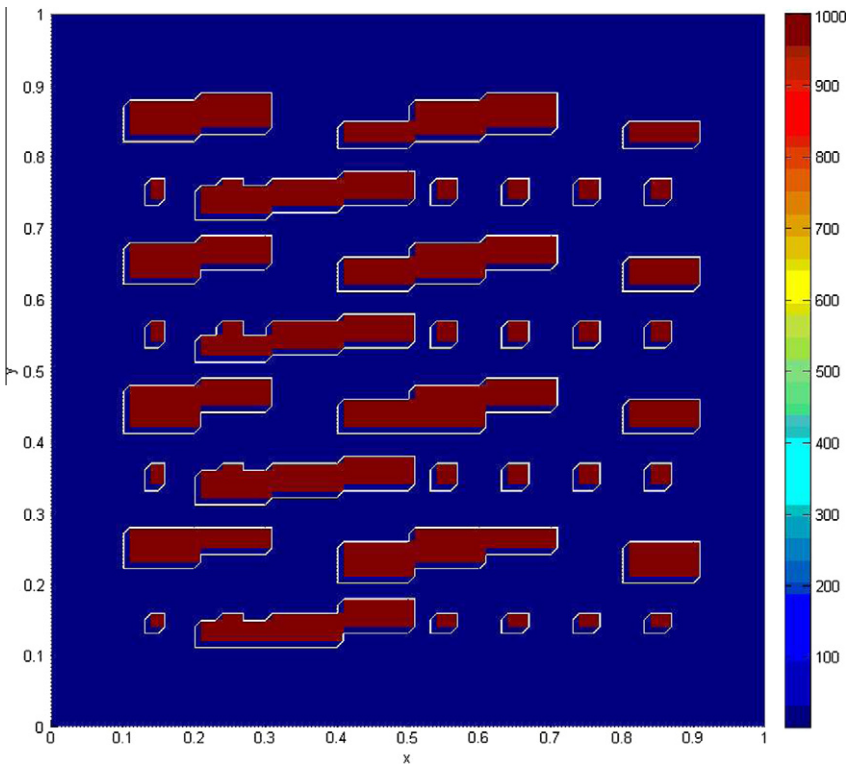

Fig. 3. Permeability field.

Table 1
The results for permeability depicted in Fig. 3. We choose HSV = 3 or HSV = 10 (in parenthesis). Here $h = 1/100,\ H = 1/10,\ \eta = 10^6$. $E^q_{r,l_2} = \|q - q_0\|^2_{l_2}/\|q\|^2_{l_2}$, $\widetilde{E^q_{r,l_2}} = \|q_0 - q^r_0\|^2_{l_2}/\|q\|^2_{l_2}$. Forcing is +1. $E^p_{w-L_2}$ is the weighted L_2 error, $E^p_{w-H^1}$ is the energy error, and $E^p_{L_2}$ is L_2 error of the solution p. The coarse space dimensions are the following. For LSM +0 is 184, for LSM +1 is 265, for LSM +2 is 346.

MS	E^q_{r,l_2}	$\widetilde{E^q_{r,l_2}}$	E^q_{tot,l_2}	$E^p_{w-L_2}$	$E^p_{w-H^1}$	$E^p_{L_2}$
LSM+0	0.119 (0.119)	0.069 (0.0077)	0.13 (0.118)	0.014	0.12	0.016
LSM+1	0.073 (0.073)	0.073 (0.015)	0.10 (0.075)	0.004	0.08	0.005
LSM+2	0.067 (0.067)	0.075 (0.015)	0.1 (0.069)	0.003	0.07	0.0046

are compared at $t = 3$. The dimensions of the coarse spaces without counting the boundary nodes are included in the captions. First column represents the relative error between fine-scale solution and coarse-scale solution for various dimensional coarse spaces. The second column represents the relative error between coarse-scale solution and reduced coarse model. The third column represents the total error. The last three columns contain errors in various norms for multiscale approximation. The notations are $E^p_{w-L_2}$ is the weighted L_2 error, $E^p_{w-H^1}$ is the energy error, and $E^p_{L_2}$ is L_2 error of the solution p. As one can see these errors decrease as we increase the dimension of the local coarse grid. As we observe from second column that a few (three) HSVs are sufficient to capture the behavior of the global coarse-scale system when the source term is 1. The relative error is about 7% and becomes less than 1% when the number of HSVs are increased to 10. We observe that the error between fine-scale solution and multiscale solution reaches 7% when we choose LSM+2, i.e., two additional basis functions per node besides those that correspond to asymptotically small eigenvalues. This indicates that coarse space should be chosen LSM+2 when three HSV's are selected. In our next numerical example, we introduce more variations into the source term which requires more global modes to achieve a high accuracy. In particular, we choose the force term to be 1 if $x > 1/2$ and -1 if $x < 1/2$. As we observe from Table 2 when using three HSV's, the error between coarse-scale system and truncated coarse-scale system is two times larger than the error between fine-scale solution and its multiscale approximation. Thus, more global coarse-scale modes are needed to balance the error between coarse-scale approximation and reduced model. We observe that when taking 10 HSVs, the error is reduced to 4 % that is about the same as LSM+2. In these examples, the output norm is L_2 and if stronger output norms are chosen, we expect more HSVs may be needed.

4.2. Example 2

In our second numerical example, we use the coefficient depicted in Fig. 4 that corresponds to a coefficient with background one and high conductivity channels and inclusions with varying conductivities within each region. In particular, we choose the high conductivities between $\eta/10$ and η randomly for each region. Here η is a fixed large number. We repeat numerical examples similar to those presented for permeability field depicted in Fig. 4. The results are presented in Tables 3 and 4. The dimensions of the coarse spaces without counting the boundary nodes are included in the captions. We select two different source terms and compare the error between multiscale approximation on a coarse grid and fine-scale solution and the error between coarse-scale approximation and the reduced model on a coarse grid. As in the first example, we observe that the error when the source term is chosen to be 1 is small when three HSVs are used to do model reduction. While the error due to coarse-scale model reduction increases when the source term has more spatial structure, such as it is equal to 1 if $x > 1/2$ and -1 if $x < 1/2$. This example shows that one needs to carefully balance the error between multiscale coarse-grid approximation and the model reduction of the coarse system. In Table 5, we show the results when the coarse-mesh size is $H = 1/20$ for the case when the forcing term is 1. We observe that with smaller coarse-mesh size, the accuracy of local model reduction method improves and, consequently, LSM+2 provides better accuracy compared to the error when only three HSV's are used (second column). We also include Fig. 5 depicting the corresponding output for the source term that is equal to 1 if $x > 1/2$ and -1 if $x < 1/2$ at $t = 3$.

4.3. Eigenvalue decay analysis

We present a result in Fig. 6 that shows the eigenvalue decay (left figure) for the fine-scale and coarse-scale systems. In this figure, the eigenvalues of fine-scale Lyapunov equation and coarse-scale Lyapunov equation are plotted for the permeability field depicted on the right figure (the computations of fine-scale HSVs for permeability fields in Figs. 3 and 4 were not

Table 2
The results for permeability depicted in Fig. 3. We choose HSV = 3 or HSV = 10 (in parenthesis). Here $h = 1/100,\ H = 1/10,\ \eta = 10^6$. $E^q_{r,l_2} = \|q - q_0\|^2_{l_2}/\|q\|^2_{l_2}$, $\widetilde{E^q_{r,l_2}} = \|q_0 - q^r_0\|^2_{l_2}/\|q\|^2_{l_2}$. Forcing is +1 if $x > 1/2$ and -1 if $x < 1/2$. $E^p_{w-L_2}$ is the weighted L_2 error, $E^p_{w-H^1}$ is the energy error, and $E^p_{L_2}$ is L_2 error of the solution p. The coarse space dimensions are the following. For LSM +0 is 184, for LSM +1 is 265, for LSM +2 is 346.

MS	E^q_{r,l_2}	$\widetilde{E^q_{r,l_2}}$	E^q_{tot,l_2}	$E^p_{w-L_2}$	$E^p_{w-H^1}$	$E^p_{L_2}$
LSM+0	0.12 (0.12)	0.23 (0.04)	0.29 (0.12)	0.003	0.12	0.016
LSM+1	0.079 (0.079)	0.25 (0.06)	0.29 (0.109)	0.002	0.08	0.007
LSM+2	0.062 (0.062)	0.26 (0.06)	0.29 (0.099)	0.002	0.06	0.005

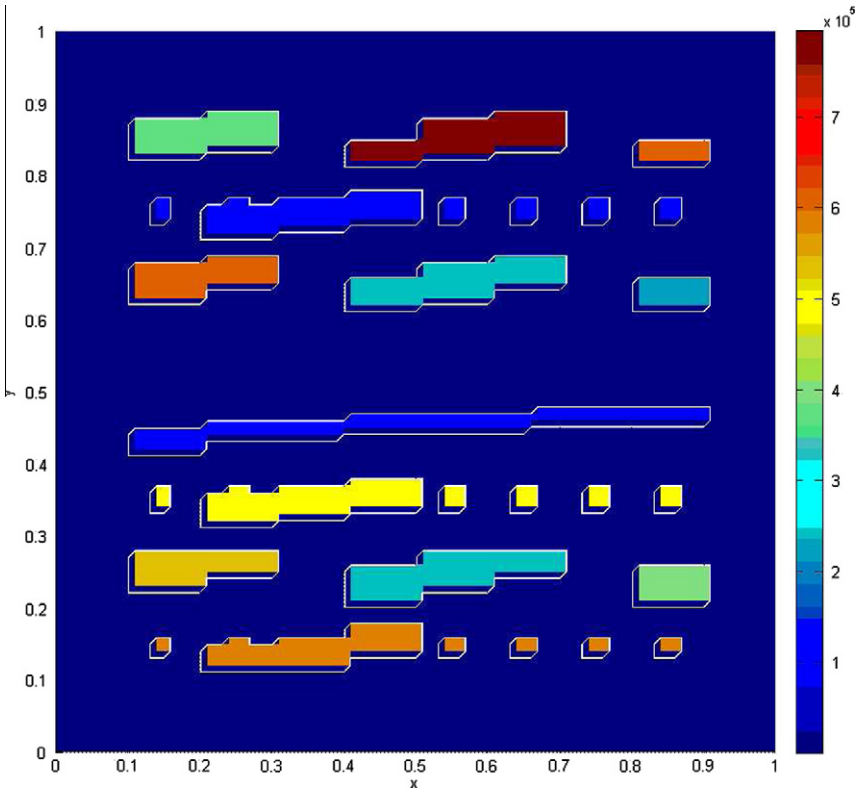

Fig. 4. Permeability field.

Table 3
The results for permeability depicted in Fig. 4. We choose HSV = 3 or HSV = 10 (in parenthesis). Here $h = 1/100,\ H = 1/10,\ \eta = 10^6$. $E^q_{r,l_2} = \|q - q_0\|^2_{l_2}/\|q\|^2_{l_2}$, $E^q_{2,l_2} = \|q_0 - q^r_0\|^2_{l_2}/\|q\|^2_{l_2}$. Forcing is +1. $E^p_{w-L_2}$ is the weighted L_2 error, $E^p_{w-H^1}$ is the energy error, and $E^p_{L_2}$ is L_2 error of the solution p. The coarse space dimensions are the following. For LSM +0 is 156, for LSM +1 is 237, for LSM +2 is 318.

MS	E^q_{r,l_2}	$\widetilde{E^q_{r,l_2}}$	E^q_{tot,l_2}	$E^p_{w-L_2}$	$E^p_{w-H^1}$	$E^p_{L_2}$
LSM+0	0.15 (0.15)	0.036 (0.0074)	0.15 (0.15)	0.022	0.134	0.022
LSM+1	0.072 (0.072)	0.062 (0.016)	0.09 (0.074)	0.0046	0.078	0.005
LSM+2	0.067 (0.067)	0.064 (0.016)	0.07 (0.07)	0.0043	0.07	0.0047

Table 4
The results for permeability depicted in Fig. 4. We choose HSV = 3 or HSV = 10 (in parenthesis). Here $h = 1/100,\ H = 1/10,\ \eta = 10^6$. $E^q_{r,l_2} = \|q - q_0\|^2_{l_2}/\|q\|^2_{l_2}$, $E^q_{2,l_2} = \|q_0 - q^r_0\|^2_{l_2}/\|q\|^2_{l_2}$. Forcing is +1 if $x > 1/2$ and −1 if $x < 1/2$. $E^p_{w-L_2}$ is the weighted L_2 error, $E^p_{w-H^1}$ is the energy error, and $E^p_{L_2}$ is L_2 error of the solution p. The coarse space dimensions are the following. For LSM +0 is 156, for LSM +1 is 237, for LSM +2 is 318.

MS	E^q_{r,l_2}	$\widetilde{E^q_{r,l_2}}$	E^q_{tot,l_2}	$E^p_{w-L_2}$	$E^p_{w-H^1}$	$E^p_{L_2}$
LSM+0	0.26 (0.26)	0.74 (0.04)	0.97 (0.27)	0.015	0.24	0.078
LSM+1	0.091 (0.091)	0.73 (0.08)	0.80 (0.14)	0.0029	0.098	0.01
LSM+2	0.072 (0.072)	0.72 (0.086)	0.78 (0.12)	0.002	0.07	0.006

possible due to our computer memory limitations). We note that in both cases, i.e., fine and coarse spaces, the eigenvalues decay fast, with the eigenvalues for the coarse space decaying slightly faster than the fine. From this figure, we see that both fine-scale and coarse-scale HSVs behave similarly and thus local–global multiscale model reduction method provides similar number of global modes as the fine-scale; however, with much less computational effort.

4.4. Discussion on computational cost

We note that for given input and output spaces, fine-scale global model reduction method provides a minimal number of basis functions for a given threshold. Using coarse spaces, one of our objectives to achieve the same dimensional global

Table 5
The results for permeability depicted in Fig. 4. We choose HSV = 3 or HSV = 10 (in parenthesis). Here $h = 1/100,\ H = 1/20,\ \eta = 10^6$. $E^q_{r,l_2} = \|q - q_0\|^2_{l_2}/\|q\|^2_{l_2}$, $\widetilde{E^q_{r,l_2}} = \|q_0 - q^r_0\|^2_{l_2}/\|q\|^2_{l_2}$. Forcing is +1. $E^p_{w-L_2}$ is the weighted L_2 error, $E^p_{w-H^1}$ is the energy error, and $E^p_{L_2}$ is L_2 error of the solution p. The coarse space dimensions are the following. For LSM +0 is 511, for LSM+1 is 872, for LSM+2 is 1233.

MS	E^q_{r,l_2}	$\widetilde{E^q_{r,l_2}}$	E^q_{tot,l_2}	$E^p_{w-L_2}$	$E^p_{w-H^1}$	$E^p_{L_2}$
LSM+0	0.13 (0.13)	0.057 (0.01)	0.13 (0.13)	0.017	0.12	0.019
LSM+1	0.03 (0.03)	0.067 (0.017)	0.071 (0.036)	0.0009	0.03	0.001
LSM+2	0.02 (0.02)	0.067 (0.018)	0.07 (0.02)	0.0004	0.02	0.0004

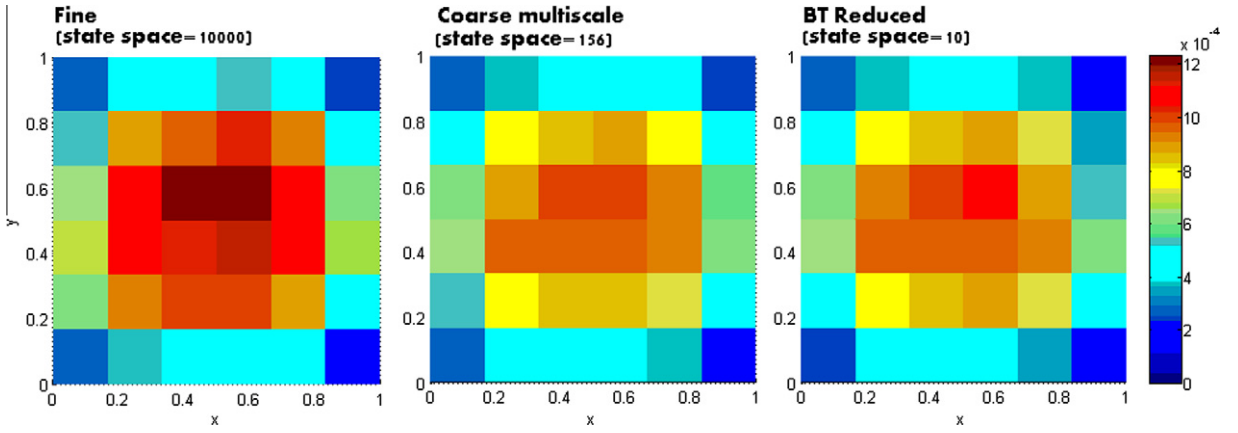

Fig. 5. Comparing output fields which correspond to average pressure fields (averaged over coarse-grid blocks). This is obtained via Cp, where $C = B^T$.

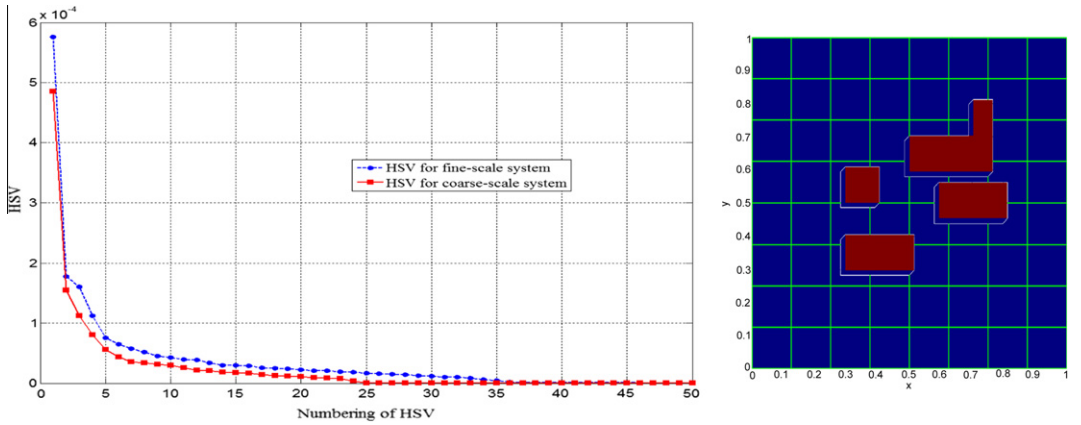

Fig. 6. Left: First 50 HSVs of the fine system (dim = 3969) and HSVs of the coarse system (dim = 65). The input space has dimension 36. Right: Coefficient used to obtain fine and coarse HSVs.

spaces without sacrificing the accuracy. For this reason, an appropriate coarse spaces are needed to balance the errors of global and local approximations. Noting that the local approximation can be improved by adding new local basis functions while global approximation can be improved by adding new global fields based on balanced truncation. Given a threshold, we need to balance these errors.

Computational efficiency of the proposed method depends on the number of coarse-grid blocks (and consequently, on the fine-grid resolution within each coarse block assuming the total number of fine degrees of freedom is fixed). One can attempt to find out an optimal number of coarse-grid blocks in order to balance the efficiency of the local approach and the global approach. This is a difficult task, in general, as it depends on the number of eigenvectors that are needed in both local and global approaches. Next, we try to obtain a simple scaling assuming that all eigenvectors are computed and the cost of solving an eigenvalue problem scales as $\mathcal{N}^3$ for $\mathcal{N} \times \mathcal{N}$ matrix. Though this estimate is not very realistic in our multiscale setup, our goal is to show that one needs to carefully choose the number of unknowns for balancing the computational efficiency of local and global approaches. Assume there are $\mathcal{M}$ coarse-grid blocks and each coarse-grid block contain $\mathcal{N}$ fine-grid blocks.

Then, the cost of the local approach scales as $\mathcal{N}^3\mathcal{M}$ while the cost of the global approach scales as $\mathcal{N}^3$. Balancing these scalings yields a specific scaling for the number of coarse-grid blocks in terms of the total fine-grid degrees of freedom. In general, one has to take into account the number of selected singular values for both local and global problems in performing these calculations and finding out the optimal scaling for the number of coarse-grid blocks. Moreover, the accuracy of local approaches can be improved by choosing non-uniform coarsening and the latter brings an additional difficulty in estimating the efficiency in terms of the number of coarse-grid blocks.

5. Conclusions

In this paper, we combine local model reduction techniques that are based on recently introduced spectral multiscale finite element methods with global model reduction methods such as balanced truncation approaches implemented on a coarse grid. Local multiscale methods considered in this paper use special eigenvalue problems in a local domain to systematically add new degrees of freedom. In these approaches, one starts with initial multiscale basis functions that contain as much local information as possible. Using the initial multiscale spaces, a local spectral problem is constructed that can add additional degrees that are missing on a coarse-grid level. Global model reduction based on balanced truncation methods is used to identify important global coarse-scale modes. The overall approach provides a substantial CPU savings as Lyapunov equations are solved for the coarse system. Compared to previous approaches where approximate models employed in global model reduction, our approaches are capable of modifying local approximate models in order to achieve a balanced error between local and global reduced models as our numerical results show. In particular, if we denote the fine-scale output by q, the coarse-scale approximation by q_0, and the reduced model coarse-scale approximation by q_0^r, we can bound the error $\|q - q_0^r\|$ as $\|q - q_0^r\| \leqslant \|q - q_0\| + \|q_0 - q_0^r\|$, where the first term is the coarse-grid approximation error that can be improved by adding local degrees of freedom and the second term is the error due to global coarse-grid approximation that can be improved by adding additional global modes.

We note that for given input and output spaces, fine-scale global model reduction method provides a minimal number of basis functions for a given threshold. Using coarse spaces, one of our objectives to achieve the same dimensional global spaces without sacrificing the accuracy. For this reason, appropriate coarse spaces are needed to balance the errors of global and local approximations. There are some important advantages in splitting the problem into local and global components. For example, if external variables (forcing, boundary conditions, nonlinearities and so on) change in time on a coarse grid, one does not need to modify basis functions. In this case, we can perform global model reduction only on a coarse grid. Note that the latter is not the case for fine-scale global model reduction methods where one needs to solve Lyapunov equations on a fine grid. We will explore these advantages in our future work, e.g., for multi-phase flow with time-dependent source terms (representing wells, cf. [9]).

Although the results presented in this paper are encouraging, there is scope for further exploration of some of the underlying approaches. As our intent here was to demonstrate that global model reduction techniques can be combined with local techniques to achieve efficient model reduction tools for high-contrast multiscale problems, we did not study the use of POD techniques and in-depth studies of thresholding procedures for local and global basis functions. In future, we also plan to study a posteriori error estimates for the proposed methods.

Acknowledgments

YE's work is partially supported by the US Army 62151-MA, DOE and NSF (DMS 0934837, DMS 0724704, and DMS 0811180). JG would like to acknowledge partial support from DOE. EG's work is partially supported by the US Army 62151-MA.

References

[1] J.E. Aarnes, On the use of a mixed multiscale finite element method for greater flexibility and increased speed or improved accuracy in reservoir simulation, Multiscale Model. Simul. 2 (2004) 421–439.
[2] J.E. Aarnes, S. Krogstad, K.-A. Lie, A hierarchical multiscale method for two-phase flow based upon mixed finite elements and nonuniform grids, Multiscale Model. Simul. 5 (2) (2006) 337–363.
[3] A.C. Antoulas, Approximation of Large-Scale Dynamical Systems, SIAM Press, Philadelphia, 2005.
[4] T. Arbogast, Implementation of a locally conservative numerical subgrid upscaling scheme for two-phase Darcy flow, Comput. Geosci. 6 (2002) 453–481.
[5] T. Arbogast, G. Pencheva, M.F. Wheeler, I. Yotov, A multiscale mortar mixed finite element method, Multiscale Model. Simul. 6 (2007) 319–346.
[6] I. Babuška, V. Nistor, N. Tarfulea, Generalized finite element method for second-order elliptic operators with Dirichlet boundary conditions, J. Comput. Appl. Math. 218 (2008) 175–183.
[7] P. Benner, J.-R. Li, T. Penzl, Numerical solution of large-scale Lyapunov equations Riccati equations and linear-quadratic optimal control problems, Numer. Linear Algebra Appl. 15 (2008) 755–777.
[8] S. Boyaval, Reduced-basis approach for homogenization beyond the periodic setting, SIAM Multiscale Model. Simul. 7 (1) (2008) 466494.
[9] M. Cardoso, L. Durlofsky, Linearized reduced-order models for subsurface flow simulation, J. Comput. Phys. 229 (3) (2010), http://dx.doi.org/10.1016/j.jcp. 2009.10.004.
[10] C.T. Chen, Linear System Theory and Design, 2nd ed., Holt, Rinehart and Winston, 1984.
[11] Y. Chen, L.J. Durlofsky, M. Gerritsen, X.H. Wen, A coupled local-global upscaling approach for simulating flow in highly heterogeneous formations, Adv. Water Resour. 26 (2003) 1041–1060.
[12] Z. Chen, T. Hou, A mixed multiscale finite element method for elliptic problems with oscillating coefficients, Math. Comput. 72 (2002) 541–576.

[13] C.C. Chu, I.G. Graham, T. Hou, A new multiscale finite element methods for high-contrast elliptic interface problem, Math. Comput. 79 (2010) 1915–1955.
[14] E. Chung, Y. Efendiev, Reduced-contrast approximations for high-contrast multiscale flow problems, Multiscale Model. Simul. 8 (2010) 1128–1153.
[15] L. Demkowicz, J. Gopalakrishnan, Analysis of the DPG method for Poisson Equation, ICES Report (2010) 10–37.
[16] J.F.M. van Doren, R. Markovinovic, J.D. Jansen, Reduced-order optimal control of water flooding using proper orthogonal decomposition, Comput. Geosci. 10 (2006) 137–158.
[17] Y. Efendiev, V. Ginting, T. Hou, R. Ewing, Accurate multiscale finite element methods for two-phase flow simulations, J. Comput. Phys. 220 (2006) 155–174.
[18] Y. Efendiev, T. Hou, Multiscale finite element methods, Theory and applications, Springer, New York, 2009.
[19] Y. Efendiev, J. Galvis, X.H. Wu, Multiscale finite element methods for high-contrast problems using local spectral basis functions, Journal of Computational Physics 230 (4) (2011) 937–955.
[20] Y. Efendiev, J. Galvis, Domain decomposition preconditioner for multiscale high-contrast problems, in: Y. Huang, R. Kornhuber, O. Widlund, J. Xu (Eds.), Domain Decomposition Methods in Science and Engineering XIX, Lecture Notes in Computational Science and Engineering, Vol. 78, Springer-Verlag, Berlin, 2011, pp. 189–196.
[21] Y. Efendiev, T. Hou, X.H. Wu, Convergence of a nonconforming multiscale finite element method, SIAM J. Num. Anal. 37 (2000) 888–910.
[22] J. Galvis, Y. Efendiev, Domain decomposition preconditioners for multiscale flows in high contrast media, Multiscale Model. Simul. 8 (2010) 1461–1483.
[23] J. Galvis, Y. Efendiev, Domain decomposition preconditioners for multiscale flows in high contrast media. Reduced dimension coarse spaces, Multiscale Model. Simul. 8 (2010) 1621–1644.
[24] I.G. Graham, R. Scheichl, Robust domain decomposition algorithms for multiscale PDEs, Numer. Methods Partial Differ. Equat. (23) (2007) 859–878.
[25] I.G. Graham, P.O. Lechner, R. Scheichl, Domain decomposition for multiscale PDEs, Numer. Math. 106 (2007) 589–626.
[26] M.A. Grepl, A.T. Patera, A posteriori error bounds for reduced-basis approximations of para- metrized parabolic partial differential equations M2AN, Math. Model. Numer. Anal. 39 (1) (2005) 157G–181.
[27] M.A. Grepl, Y. Maday, N.C. Nguyen, A.T. Patera, Efficient reduced-basis treatment of nonaf- fine and nonlinear partial differential equations M2AN, Math. Model. Numer. Anal. 41 (2) (2007) 575G–605.
[28] M. Heinkenschloss, T. Reis, A.C. Antoulas, Balanced truncation model reduction for systems with inhomogeneous initial conditions, Automatica 47 (2011) 559–564.
[29] J.P. Hespanha, Linear Systems Theory, Princeton University Press, 2009.
[30] T. Hou, X.H. Wu, A multiscale finite element method for elliptic problems in composite materials and porous media, J. Comput. Phys. 134 (1997) 169–189.
[31] P. Jenny, S.H. Lee, H. Tchelepi, Multi-scale finite volume method for elliptic problems in subsurface flow simulation, J. Comput. Phys. 187 (2003) 47–67.
[32] T. Kailath, Linear Systems, Prentice-Hall, New Jersey, 1980.
[33] S. Krogstad, A Sparse Basis POD for model reduction of multiphase compressible flow, SPE 141973, This paper was prepared for presentation at the 2011 SPE reservoir simulation symposium held in The Woodlands, Texas, USA, 21G23 February 2011.
[34] I. Lunati, P. Jenny, Multi-scale finite-volume method for highly heterogeneous porous media with shale layers, in: Proc. 9th Euro. Conf. on Mathematics of Oil Recovery (ECMOR), 2004, Cannes, France.
[35] Y. Maday, A.T. Patera, G. Turinici, Global a priori convergence theory for reduced-basis approximations of single-parameter symmetric coercive elliptic partial differential equations, C.R. Acad. Sci. Paris Ser. I 335 (3) (2002) 289G294.
[36] H. Owhadi, L. Zhang, Metric based up-scaling, Comm. Pure Appl. Math. LX (2007) 675–723.
[37] E.D. Sontag, Mathematical Control Theory. Deterministic Finite Dimensional Systems, Text in Applied Mathematics, 2nd ed., 6, Springer-Verlag, New York, 1998.
[38] T. Strouboulis, I. Babuška, K. Copps, The design and analysis of the generalized finite element method, Comput. Methods Appl. Mech. Engrg. 181 (2000) 43–69.
[39] P.S. Vassilevski, Multilevel Block Factorization Preconditioners, Matrix-Based Analysis and Algorithms for Solving Finite Element Equations, Springer, New York, 2008.
[40] P.S. Vassilevski, Coarse spaces by algebraic multigrid: multigrid convergence and upscaled error estimates, submitted for publication.
[41] S. Volkwein, Proper orthogonal decomposition surrogate models for nonlinear dynamical systems: error estimates and suboptimal control, in: P. Benner, V. Mehrmann, D.C. Sorensen (Eds.), Reduction of Large-Scale Systems, Lecture Notes in Computational Science and Engineering, 45, 2005, pp. 261–306.
[42] K. Zhou, J.C. Doyle, K. Glover, Robust and Optimal Control, Prentice Hall, Englewood Cliffs, NJ, 1996.